Bulletin of Engineering Geology and the Environment (2023) 82:296
https://doi.org/10.1007/s10064-023-03295-0

ORIGINAL PAPER

Strength, deformation, and failure characteristics of hollow cylinder sandstone under axial–torsional tests

Yue Jiang[1,2] · Hui Zhou[2,3] · Jingjing Lu[2,3] · Yang Gao[2,3] · Zhen Li[4]

Received: 14 November 2022 / Accepted: 2 June 2023 / Published online: 5 July 2023

Abstract

Due to the excavation disturbance in deep tunnel, the stress magnitude and orientation changed obviously, which affects the mechanical properties of surrounding rock and the stability of tunnel. The axial–torsional test is adopted to study the influence of stress orientation on the strength and deformation behavior of four sandstones, using the self-developed hollow cylinder torsional apparatus for rock. The results show that the peak shear strength of sandstone is nonlinear, positively correlated with axial stress, and negatively correlated with the rotation angle of the principal stress axis. The stress–strain curve obtained under the rotation of principal stress axis can be divided into compaction, elasticity, yield, and softening stages. Furthermore, the sensitivity of the crack damage threshold of various sandstone is analyzed. The results show that the rotation of the principal stress axis can aggravate rock damage, and the greater the initial damage degree, the stronger the impact. Finally, the evolution mechanism of the internal rock cracks under the axial–torsional test is discussed by analyzing the rock failure characteristics, and it can be seen that the initiation, propagation, and coalescence of cracks are not only affected by stress magnitude, but also the stress orientation. Moreover, the crack propagation model considering principal stress axis rotation is verified and improved experimentally. The results of this research are of great significance to studying the influence of stress orientation and provide an important method to investigate the mechanical properties of rock with complex stress states comprehensively.

Keywords Axial–torsional test · Hollow cylinder sandstone · Principal stress axis rotation · Rock strength · Deformation characteristics · Crack propagation

Abbreviations

$_c$	Cohesion
φ	Internal friction angle
F	Axial force
M_t	Torque
σ_c	The uniaxial compression strength
σ_z	Axial stress
σ_θ	Circumferential stress
$\tau_{z\theta}$	Shear stress
$\gamma_{z\theta}$	Shear strain
σ_1	The maximum principal stress
σ_2	The intermediate principal stress
σ_3	The minimum principal stress
α	Principal stress rotation angle
p	Mean stress
q_J	Generalized shear stress
γ_g	Generalized shear strain
n	Axial compression ratio
L	Length of the torque arm
D	Diameter of the axial loading piston
R	Radius of the piston in the torque hydraulic jack

✉ Hui Zhou
hzhou@whrsm.ac.cn

[1] Suzhou University of Science and Technology, Suzhou 215000, Jiangsu, China

[2] State Key Laboratory of Geomechanics and Geotechnical Engineering, Institute of Rock and Soil Mechanics, Chinese Academy of Sciences, Wuhan 430071, Hubei, China

[3] University of Chinese Academy of Sciences, Beijing 100049, China

[4] Henan Polytechnic University, Jiaozuo 454000, Henan, China

Introduction

With the rapid development of the social economy in recent years, the demand for the development and utilization of underground space has never been as strong. A large number of deep-rock-mass projects have emerged in many fields,

such as the exploitation of mineral resources, the construction of large-scale underground caverns for hydropower projects, the development of oil and gas, the deep buried disposal of nuclear waste, and the utilization of geothermal energy. The ensuing complex geological environment and specialized construction techniques have led to new scientific breakthroughs in the deformation and destruction of surrounding rocks (Qian and Li 2008). Consequently, it has become increasingly necessary to explore the mechanical properties of rocks in complex environments.

Sandstone, one of the most common geological rock bodies in deep buried underground engineering, has been studied by many scholars who have produced rich research results. The basic mechanical properties of sandstone have been thoroughly studied based on conventional rock mechanics. With the improvement of test technology, the stress state that can be achieved by test equipment has become increasingly complicated, and scholars now have a better understanding of the mechanical properties of sandstone. Feng et al. (2004) studied the damage evolution law of sandstone under triaxial compression with chemical corrosion based on CT test technology. Wasantha et al. (2015) provided the effects of strain rate and grain size on the mechanical response characteristics of sandstone under the uniaxial compression test, and the fine-grained (FG) was considered the most sensitive to strain rate. Yang (2016) and Yang et al. (2012) (Yang and Jing 2013; Yang et al. 2015; 2017) used various test methods to research sandstone to analyze its strength, deformation, and failure characteristics. Through conventional compression and indirect tensile tests, the mechanical properties of sandstone with bedding surfaces were studied, and the stress level and structural anisotropy were considered the most significant factors (Hu et al. 2017). Wang et al. (2017) proposed a mechanical model which can describe its elastoplastic behavior based on the strength and deformation characteristics of sandstone under triaxial compression. Li et al. (2020a, b) adopted an energy-based fatigue damage model to describe the energy evolution law and fatigue behavior characteristics of sandstone under the uniaxial cyclic compression test. With the progressive development of research, the dynamic characteristics of sandstone are gradually being considered. Li et al. (2008; 2017) conducted an experimental study on the impact of the same dynamic load under different axial compressions and the critical impact failure of rocks under different axial compressions.

In recent years, with the emergence of nuclear waste disposal, geothermal development, oil and gas exploitation, and other projects, many scholars have focused on the mechanical behavior and seepage characteristics of sandstone under multifield coupling (temperature, chemistry, stress, and seepage) (Logan and Blackwell 1983; Feucht and Logan 1990; Dunning et al. 1994; Hu et al. 2010; Xu and Yang 2016; Li et al. 2020a, b). Researchers have found that the stress state of the surrounding rock in deep engineering often suffers from the rotation of the principal stress axis under the influence of excavation disturbance, meaning that the mechanical properties of the surrounding rock are affected by both the magnitude and orientation of the stress (Abel and Lee 1973; Lee et al. 1999; Diederichs 2000; Eberhardt 2001; Kaiser et al. 2001; Alsayed 2002; Diederichs et al. 2004; Zhang et al. 2013; Jiang et al. 2019, 2023). Although scholars have obtained rich results in the study of sandstone, their focus has been on the impact of stress or external environmental changes on the mechanical behavior of sandstone, ignoring the effect of stress orientation. Accurately describing the strength, deformation, and failure of rock masses is the theoretical basis for engineering safety and stability evaluation. The self-developed hollow cylinder torsional apparatus for rock (Zhou et al. 2018a, 2018b) can realize the complex stress path including the change of stress orientation, and the reliable results have been obtained in previous work. In this research, a series of axial–torsional tests are conducted on four types of sandstone to investigate the effect of the stress orientation on the strength, deformation and failure characteristic of rock. First, the strength, deformation, and failure characteristics of sandstone under the rotation of the principal stress axis are obtained by analyzing the relationship between the axial-stress–shear-stress, stress–strain, and macroscopic failure. Then, the effect of the initial damage degree is explored based on the strength and deformation behavior of the rock under different axial stress levels. Finally, the mechanism of microscopic crack evolution with different sandstones is analyzed, considering the influence of stress orientation.

Experimental methods

Specimen

To study the mechanical characteristics of different sandstone under combined axial and torsional loads, red sandstone, white sandstone, fine gray sandstone, and coarse gray sandstone were used to conduct experiments. All four sandstones were sourced from Sichuan Province, China, with uniform texture and no obvious defects. According to the results of previous studies (Hight et al. 1983; Vaid et al. 1990; Sayao and Vaid 1991), combined with the characteristics of the rock, the size of the hollow cylinder specimen is finally determined to be 50 mm (outer diameter), 30 mm (inner diameter), and 120 mm (length). As shown in Fig. 1, the hollow cylinder specimens were cored from the same block of material using a double-drill coring system, which can drill the outer and inner bores simultaneously (Zhou et al. 2018a). According to X-ray diffraction (XRD) test results, the main minerals in sandstone are quartz, albite, microcline, kaolinite, calcite, and illite, as listed in Fig. 1. In addition, the basic mechanical parameters of four sandstones are obtained by conventional

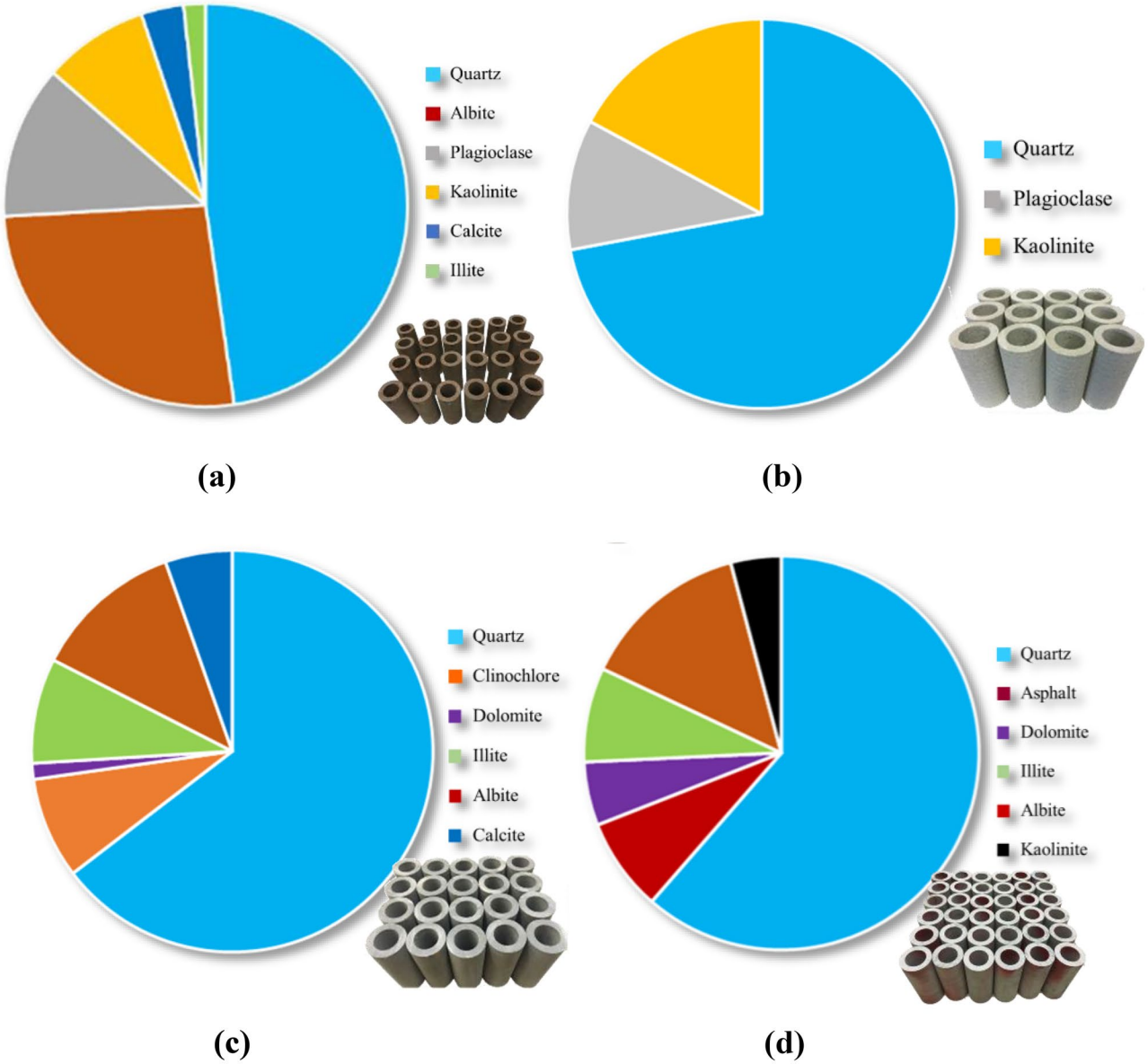

Fig. 1 The mineral composition of different types of sandstone: **a** red sandstone; **b** white sandstone; **c** fine gray sandstone; **d** coarse gray sandstone

rock mechanics tests, as listed in Table 1. In this table, σ_c is the uniaxial compressive strength (UCS) under uniaxial compression, and c and φ are the cohesion and friction angle under the direct shear test, respectively.

Testing scheme and procedure

The axial–torsional tests are conducted by self-developed hollow cylinder torsional apparatus for rock which can realize the axial force, torque, and internal and external confining pressures loaded simultaneously (Zhou et al. 2018a). As shown in Fig. 2, the test system consists of high-precision servo loading control systems, a torque-applying device, an axial loading piston, a triaxial cell, and a data acquisition device. The specimen is bonded to the top

Table 1 Mechanics parameters for different types of sandstone

Rock types	σ_c/MPa	c/MPa	φ/(°)	σ_z /MPa
Red sandstone	40	9	28.83	0/5/10/15/20/25/30
White sandstone	36	8.25	42.55	2/5/10/15/20/25/30
Gray sandstone (fine)	90	13.19	41.48	5/20/40/50/60/70/80/85
Gray sandstone (coarse)	70	23.9	35	5/10/20/30/40/50/60

and bottom loading units with epoxy sealant, and then placed into the triaxial cell. The axial force is applied to the specimen through the axial loading piston up and down movements, and the torque is transmitted by the torque-applying device and the tenon structure. And the inner and outer walls of the specimen are sealed to achieve the application of internal and external confining pressures. High-precision servo loading control systems with a maximum axial force and torque loading capacity of 400 MPa and 330 MPa are adopted, respectively, and LVDTs and outer and inner strain rings are used to measure the deformation of the specimen, which was previously described in the studies (Zhou et al. 2018a). This study mainly focuses on the axial force and torque, and the specific expressions are illustrated in Eqs. 1 ~ 7.

$$\sigma_z = \frac{F \cdot \left(D^2/4 - r_0^2\right)}{r_0^2 - r_i^2} \tag{1}$$

$$\tau_{z\theta} = \frac{3M_t R^2 L}{2\left(r_0^3 - r_i^3\right)} \tag{2}$$

$$\alpha = \frac{1}{2}\arctan\frac{2\tau_{z\theta}}{\sigma_z} \tag{3}$$

$$\sigma_1 = \sigma_z/2 + \sqrt{\sigma_z^2/4 + \tau_{z\theta}^2} \tag{4}$$

$$\sigma_3 = \sigma_z/2 - \sqrt{\sigma_z^2/4 + \tau_{z\theta}^2} \tag{5}$$

$$p = \frac{1}{3}\left(\sigma_1 + \sigma_3\right) \tag{6}$$

$$q_J = \frac{1}{\sqrt{2}}\sqrt{\sigma_1^2 + \sigma_3^2 + \left(\sigma_3 - \sigma_1\right)^2} \tag{7}$$

The specific loading path is shown in Fig. 3. The process (O–A) means that the axial force F is loaded to a predetermined value and the rotation angle α is 0. And then, a torque M_t is applied at an oil discharge rate of 1 mL/min until the sample is damaged (A–B'–B''); among them the rotation angle increases gradually (0–α'–α''). To study the influence of initial damage degree, different stress levels were selected for loading, and the corresponding axial stress application level was determined based on the uniaxial compressive strength of the different types of sandstone (Table 1). To obtain more reliable test results for different rock types, three sets of parallel tests were conducted for each test condition, and the average of the results was selected for data analysis.

Experimental results

Analysis of strength during the rotation of principal stress axis

To analyze the strength characteristics of various types of sandstone under axial–torsional test conditions visually and comprehensively, the characteristics of the deviated plane (axial stress vs. shear stress) and the principal stress plane

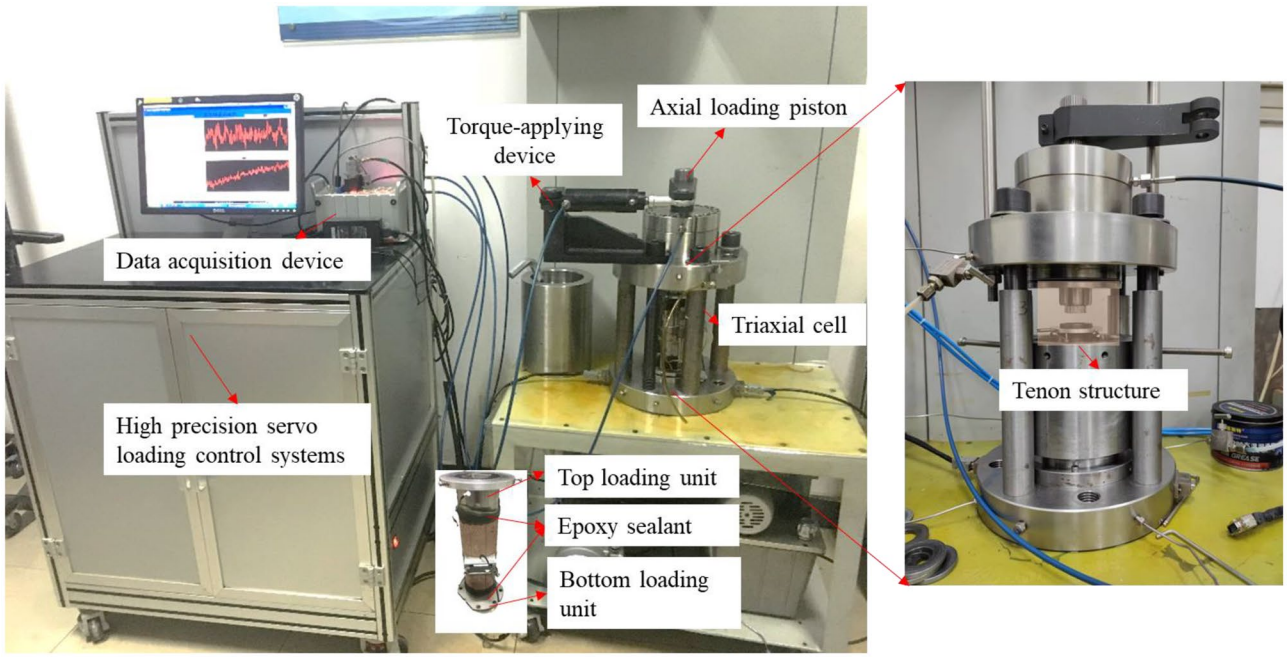

Fig. 2 Illustration of the hollow cylinder torsional apparatus for rock (HCAR)

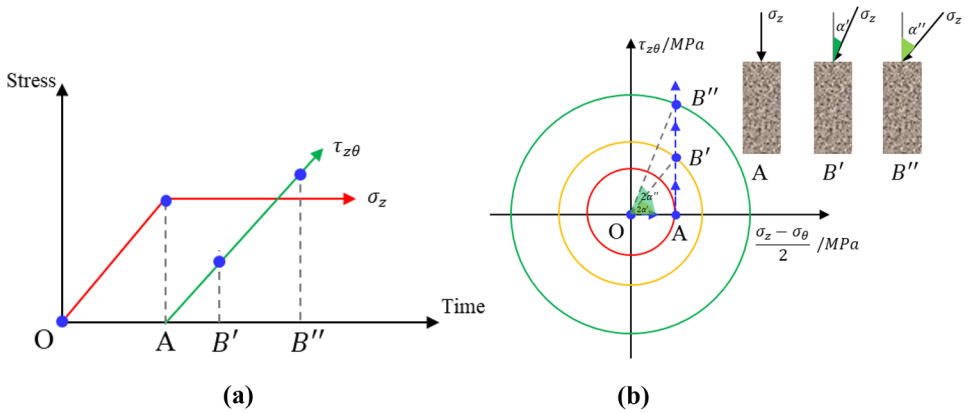

Fig. 3 Stress path under axial–torsional test: **a** schematic diagram of experiment loading path; **b** stress path on the deviatoric stress plane ($(\sigma_z - \sigma_\theta/2)$ -$\tau_{z\theta}$)

(mean stress, generalized shear stress, and principal stress axis rotation angle) were investigated. The above parameters can be calculated by Eqs. 1 ~ 7.

Observing the axial stress vs. shear stress curves in Fig. 4a, it is clear that the peak strengths of four sandstones increase nonlinearly with axial stress, the incremental amplitude being gradually reduced. When the axial stress is minor, a slight increase in it causes the shear strength of the rock to increase rapidly. As the axial stress increases, the growth slope rapidly decreases. Under conditions of larger axial stress, the shear strength of the obtained fine gray sandstone is relatively discrete. This change is the same as that of the conventional rock mechanics test, confirming the reliability of the basic principle of the axial–torsional test. In the principal stress plane (Fig. 4b,c), the mean stress and generalized shear stress show a nearly linear positive correlation, whereas the rotation angle of the principal stress axis decreases with increasing mean stress, being approximately a quadratic parabola function. This law was consistently reflected in the four sandstones.

To further analyze the relationship between the rotation angle of the principal stress axis and the mean stress, the process can be divided into two stages based on the slope change trends (Fig. 4c, Table 2). In stage I, the rotation angle of the principal stress axis of each sandstone decreases rapidly with an increase in the mean stress until stage II the change is tiny, gradually tending toward a specific value. The critical mean stress values of each sandstone (red sandstone (5 MPa), white sandstone (8 MPa), fine gray sandstone (16.6 MPa), and coarse gray sandstone (10 MPa)) can be found by analyzing the curve variation characteristics in Fig. 4c. According to Eq. 6, the corresponding critical axial stresses are 15 MPa, 24 MPa, 49.8 MPa, and 30 MPa, respectively. Furthermore, the variation amplitude of the rotation angle of the principal stress axis at different stages can be obtained from Fig. 4c, as shown in Table 2. Combining the uniaxial compressive strength of each sandstone, it was found that the critical stress value of each rock increased approximately in line with its increasing uniaxial compressive strength—fine gray sandstone > coarse gray sandstone > white sandstone > red sandstone, meaning that the critical stress value was closely related to the properties of the rock materials, the mechanism of which is discussed in detail below.

Analysis of strain during the rotation of principal stress axis

Different from the conventional solid cylinder, corresponding axial strain, hoop, radial, and shear strains are generated simultaneously under the axial force and torque with a hollow cylinder specimen. To comprehensively study the deformation characteristics of rock, based on experimental principles combined with the strength analysis method, the shear-stress–shear-strain coordinate system and the generalized shear stress-generalized shear strain coordinate system were selected. The test data of different axial stress levels (red sandstone (5.01 MPa, 14.97 MPa, 25 MPa, and 29.88 MPa), white sandstone (4.92 MPa, 9.79 MPa, 19.88 MPa, and 29.53 MPa), fine gray sandstone (5.16 MPa, 19.45 MPa, 39.94 MPa, and 84.4 MPa), and coarse gray sandstone (5.1 MPa, 20.27 MPa, 40.49 MPa, and 60.26 MPa)) were plotted in two coordinate systems (see Fig. 5).

In the shear-stress–shear-strain coordinate system, the shear strain increases with increasing shear stress. When the shear stress reaches a specific value, it exhibits an obvious strain softening phenomenon, especially the larger axial stress applied. Furthermore, with increases in axial stress, the shear strain of red and coarse gray sandstone was relatively small, even decreasing in the white sandstone, while the fine gray sandstone exhibited a trend of decreasing shear strain initially, before increasing. It is because, compared with the other three rock types, the uniaxial compressive strength and brittleness of fine gray sandstone were higher, exhibiting clear brittleness under smaller axial stress, while the ductility characteristics changed slowly under larger axial stress.

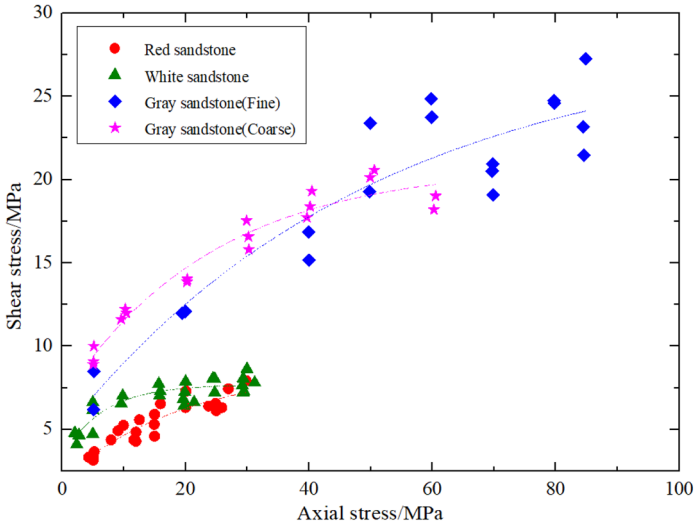
Red sandstone
White sandstone
Gray sandstone(Fine)
Gray sandstone(Coarse)
Shear stress/MPa
Axial stress/MPa

(a)

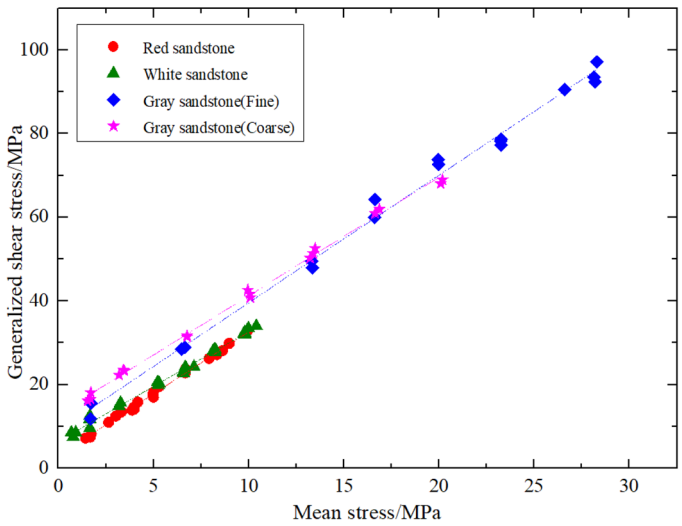
Red sandstone
White sandstone
Gray sandstone(Fine)
Gray sandstone(Coarse)
Generalized shear stress/MPa
Mean stress/MPa

(b)

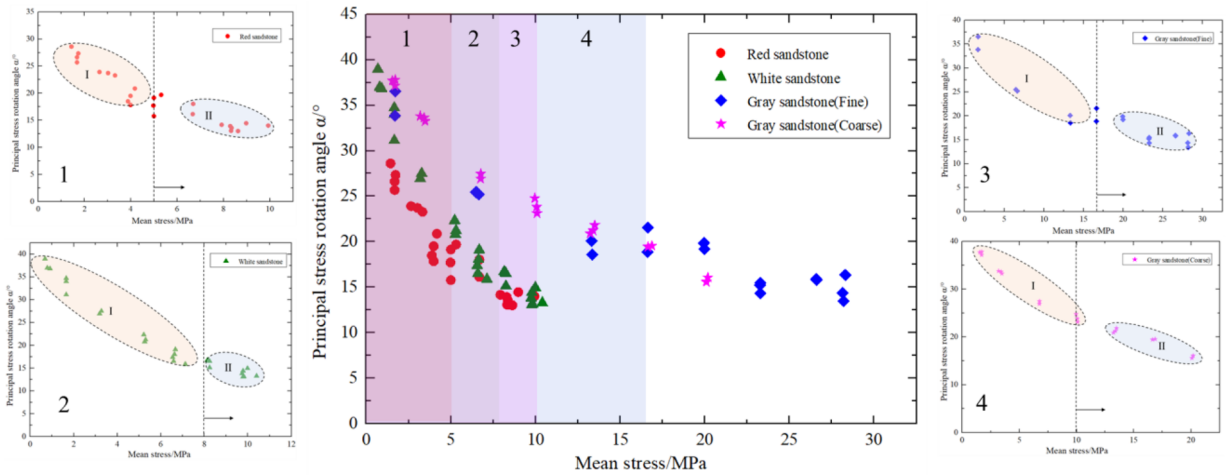
1
2
3
4
Red sandstone
White sandstone
Gray sandstone(Fine)
Gray sandstone(Coarse)
Principal stress rotation angle α/°
Mean stress/MPa

(c)

◂**Fig. 4** Strength curves of different types of sandstone under axial–torsional test: **a** axial stress VS shear stress (cylindrical coordinate system); **b** mean stress VS generalized shear stress (Cartesian coordinate system); **c** mean stress VS principal stress rotation angle (Cartesian coordinate system)

In contrast to the various characteristics of shear-stress–shear-strain, the generalized shear strain of each sandstone increases significantly with increasing axial stress. The generalized shear strain is a comprehensive concept, and the rock undergoes greater deformation in the axial, radial, and circumferential directions under larger axial stress. In addition, similar to the conventional stress–strain curve—the generalized shear stress-generalized shear strain curve of the sandstone under axial–torsional test conditions could also be divided into four stages: the initial compaction stage, elastic stage, yielding stage, and strain softening stage. That is to say, cracks in rock undergo compaction, stable expansion, unstable expansion, and even transfixion under the principal stress axis rotation. Moreover, the deformation modulus increases gradually and the yield stage of different sandstone becomes more obvious with the increase of axial stress. That means more energy is stored inside the rock under high stress conditions, considering the principal stress axis rotation for the same deformation. It can be seen that white sandstone does not entirely conform to the above laws, due to its larger grain size and lower strength. In summary, the generalized-shear-stress–generalized-shear-strain should be selected to analyze the rock deformation behavior under the change of stress orientation, and the curve describes the evolution of rock crack propagation.

Macroscopic failure characteristic

The failure of the rock during loading is the macroscopic expression of its internal forces. This section analyzes the influence of the principal stress axis rotation on the characteristics of failure. Limited by the length of the paper, this section analyzes several failure specimens under typical axial stress for each type of sandstone (Fig. 6). The red dotted line in the sample failure diagram indicates the fracture surface of the specimen.

As shown in Fig. 6, the failure mode of red sandstone and white sandstone under low axial stress is an oblique shear crack through the upper and lower ends of the specimen. When the axial stress is higher, the failure mode is transformed into an oblique shear main crack, accompanied by several secondary tensile cracks. The failure modes of coarse gray sandstone with axial stress are similar to those of red sandstone and white sandstone, the difference being that the failure under higher axial stress is more severe. Unlike the three sandstones, the shear failure of fine gray sandstone under low axial stress only occurs in the middle area of the sample. As the axial stress increases, the failure area gradually expands to both ends of the specimen and generates several tensile cracks, the degree of damage increasing progressively, with even the phenomenon of rock ejection appearing. The reason is that fine gray sandstone has high and clear brittleness, especially under higher axial stress, which releases large amounts of energy at the moment of failure, resulting in severe damage. Thus, with an increase in axial stress under the axial–torsional test, the failure modes of the four sandstones gradually changed from shear failure to tensile-shear failure, and the degree of damage became increasingly severe.

Discussion

Effect of initial damage degree on rock mechanical properties under rotation of principal stress axis

The current research results show that the initial damage degree of rock has an essential impact on its deformation and failure (Zou and Kaiser 1990; Yi et al. 2017). This study explores the influence of principal stress orientation on rock mechanical behavior under different initial damage degree by applying different axial stresses. The axial compression ratio n was selected for quantitative analysis—that is, the ratio of axial stress to uniaxial compressive strength (Eq. 8). It not only reflects the damage degree of the rock at different axial stress levels but also characterizes the initial stress state of the rock. Moreover, it can normalize the test results of the four sandstones, which is conducive to obtaining universal

Table 2 The critical mean stress and axial stress of four sandstones

Rock types	I		II	
	p/MPa (σ_z/MPa)	α/°	p/MPa (σ_z/MPa)	α/°
Red sandstone	$p \le 5(\sigma_z \le 15)$	30° ~ 17°	$P > 5(\sigma_z > 15)$	17 ~ 14°
White sandstone	$p \le 8(\sigma_z \le 24)$	40° ~ 16°	$p > 8(\sigma_z > 24)$	16 ~ 13°
Gray sandstone (fine)	$p \le 16.6(\sigma_z \le 49.8)$	35° ~ 20°	$p > 16.6(\sigma_z > 49.8)$	20 ~ 15°
Gray sandstone (coarse)	$p \le 10(\sigma_z \le 30)$	35° ~ 22°	$p > 10(\sigma_z > 30)$	22 ~ 15°

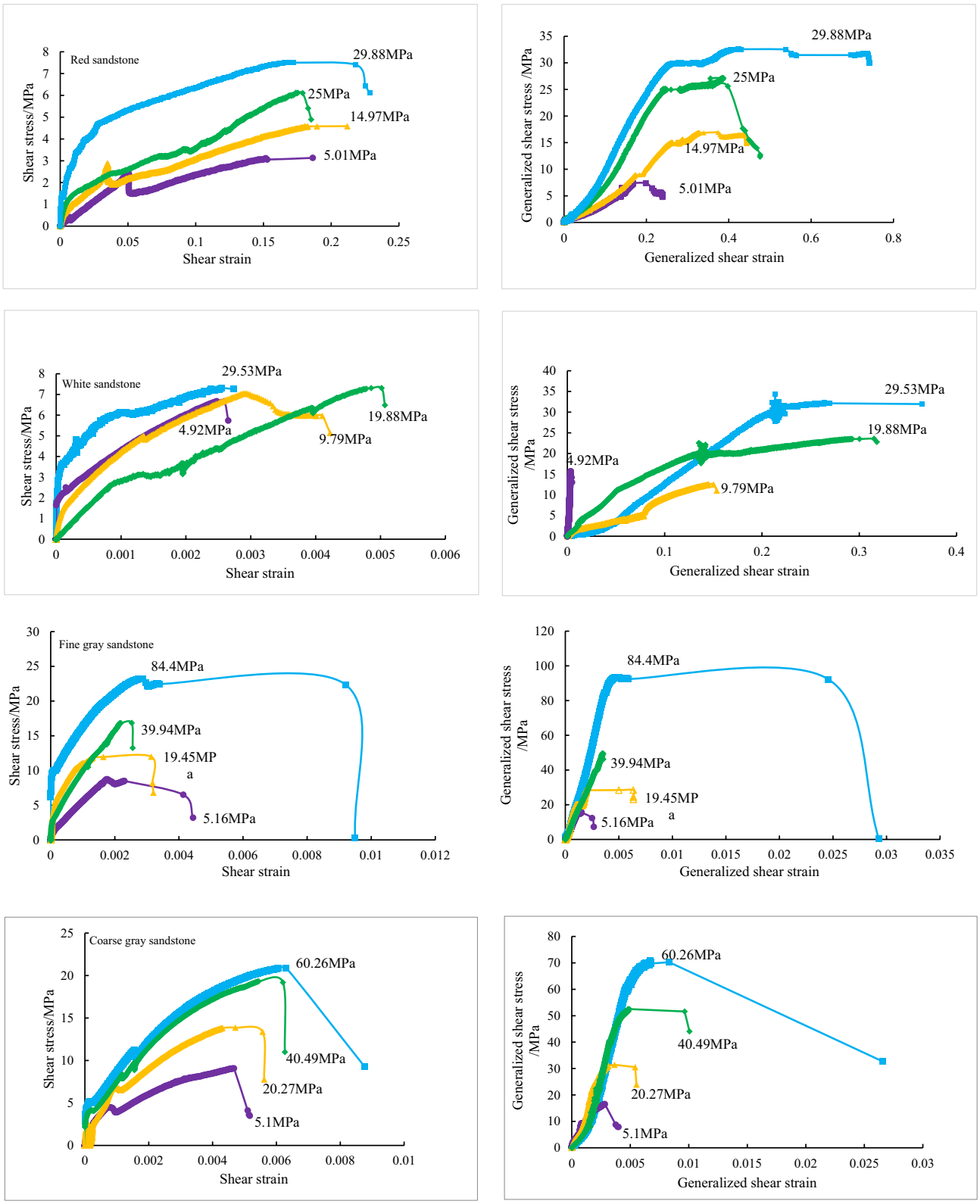

Fig. 5 Deformation curves of different types of sandstone under axial–torsional test. Shear stress VS shear strain (cylindrical coordinate system); generalized shear stress VS generalized shear strain (Cartesian coordinate system)

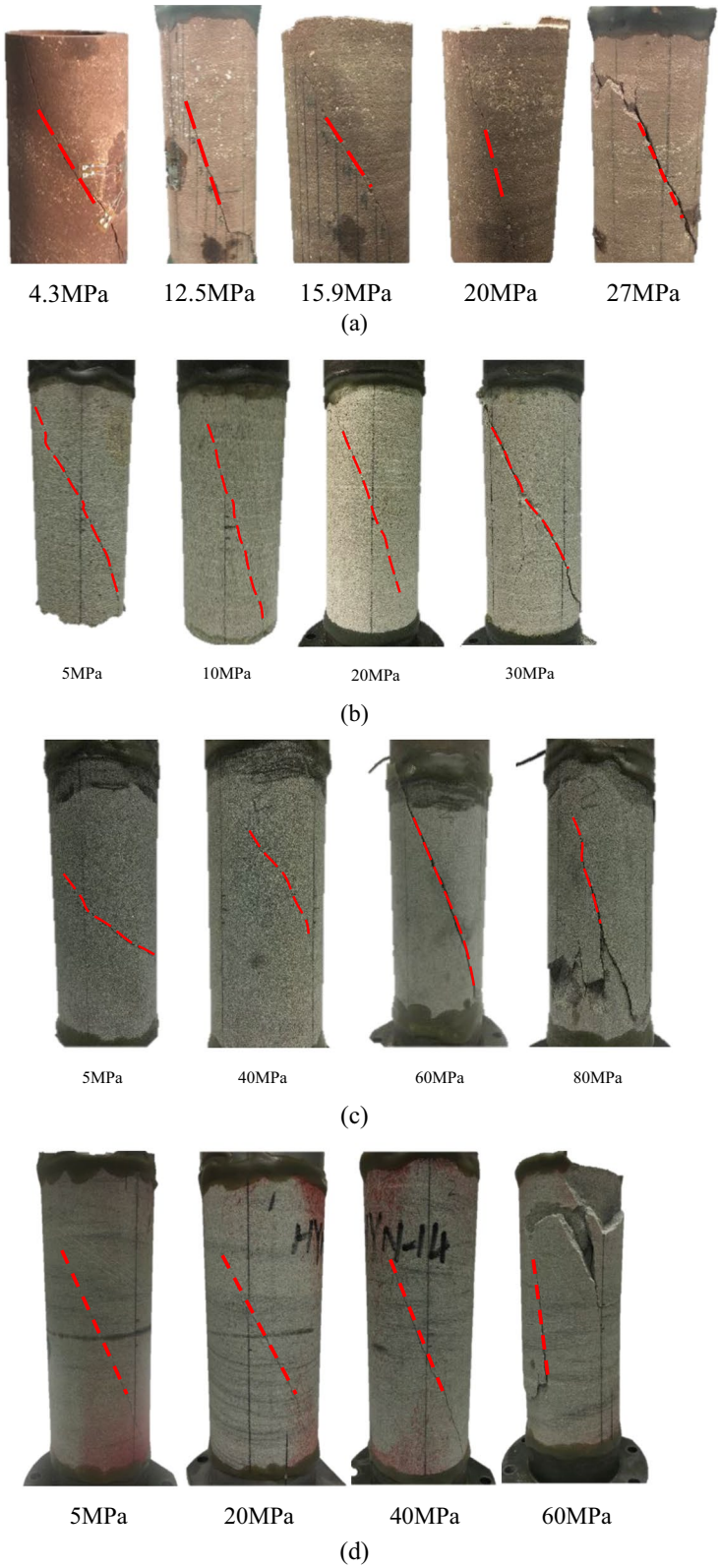

Fig. 6 Failure characteristics of sandstones under axial–torsional test. **a** Red sandstone; **b** white sandstone; **c** fine gray sandstone; **d** coarse gray sandstone

laws. Consequently, this section analyzes the relationship between the axial compression ratio of each sandstone and the shear stress, the generalized shear stress, and the rotation angle of the principal stress axis, as shown in Fig. 7.

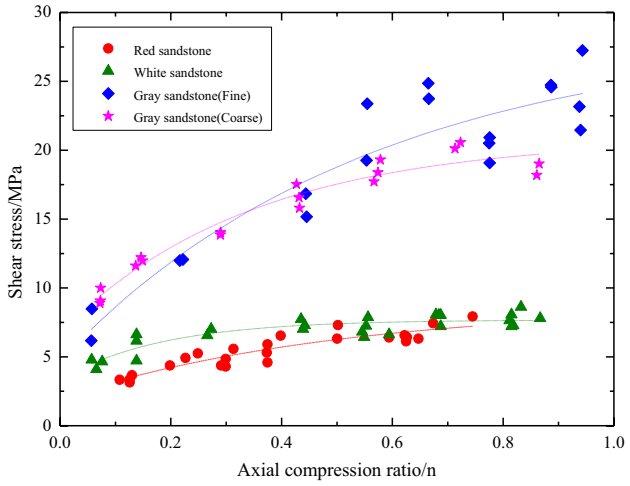

(a)

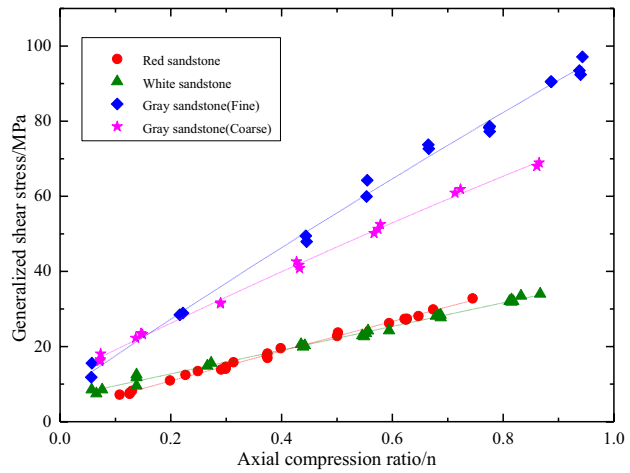

(b)

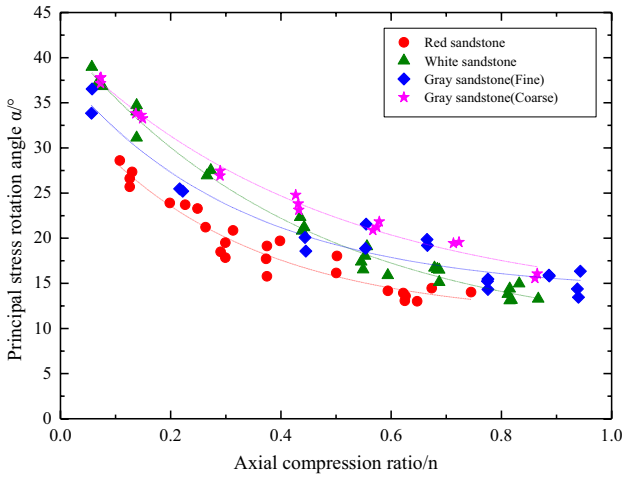

(c)

Fig. 7 The relationship between the axial compression ratio, the shear stress, generalized shear stress, and the rotation angle of the principal stress axis: **a** axial compression ratio VS shear stress; **b** axial compression ratio VS generalized shear stress; **c** axial compression ratio VS principal stress rotation angle

$$n = \frac{\sigma_z}{\sigma_c} = \frac{3p}{\sigma_c} \tag{8}$$

The growth rate of the shear stress and generalized shear stress with the axial compression ratio increase is illustrated in Table 3. It was found that the shear stress and generalized shear stress of sandstone under the axial–torsional test condition both increased with an increasing axial compression ratio and the higher the rock strength, the greater the increase. This law is similar to the confining pressure effect in conventional triaxial tests. The larger the initial stress of the rock, the stronger the bearing capacity—that is, the high-stress environment improves the bearing capacity of the rock to a certain extent, even under the condition of principal stress rotation.

Compared with the conventional rock mechanics test, the axial–torsional test realizes the continuous rotation of the principal stress axis, so it is necessary to explore the relationship between the principal stress axis rotation angle and the axial compression ratio. Figure 7c shows the relationship between the axial compression ratio of each sandstone and the rotation angle of the principal stress axis. It was found that:

1) A nonlinear-fitting ($\alpha = a - b \bullet c^n$) with a high correlation coefficient ($R^2 = 0.93 \sim 0.99$) is employed as shown in Table 4. The principal stress axis rotation angle corresponding to each sandstone decreases nonlinearly with an increasing axial compression ratio, the decreasing trend gradually slowing down.
2) When the axial compression ratio is less than 0.6, the higher the strength of the sandstone, the larger the corresponding principal stress axis rotation angle when it fails.

This feature is particularly significant at lower axial compression ratios. What is the significance of these laws? How do they help us understand the influence of the initial stress state on the mechanical properties of the rock under the rotation of the principal stress axis? The author believes that it should be combined with Sec. 3.1, to conduct a comprehensive analysis from an energy point of view. As mentioned above, the mean stress of each sandstone in the principal stress plane is related to the rotation angle of the stress axis, and there is a critical mean stress value (as obtained in Sec. 3.1) that divides the curve into two stages, and which can be converted into a critical axial compression ratio by using Eq. (8), as summarized in Table 5.

The critical axial compression ratio of each sandstone was between 0.4 and 0.6. Specifically, when n was less than 0.4, the rotation angle of the principal stress axis decreased significantly with an increase in the axial stress. When n was greater than 0.6, the angle did not change significantly. These results were consistent with the results obtained above, showing that it is feasible to characterize sandstone

Table 3 The growth rate of the shear stress and generalized shear stress of four sandstones

Rock types	n	$\tau_{z\theta}$/MPa	The growth rate of $\tau_{z\theta}$	q_1 /MPa	The growth rate of q_1
Red sandstone	0.1 ~ 0.75	3.3 ~ 7.9	139%	7.2 ~ 32.8	356%
White sandstone	0.06 ~ 0.87	4.8 ~ 7.8	62.5%	8.5 ~ 34	300%
Gray sandstone (fine)	0.06 ~ 0.94	8.5 ~ 21.5	153%	15.6 ~ 92.4	492%
Gray sandstone (coarse)	0.07 ~ 0.87	8.9 ~ 19.0	113.5%	16.1 ~ 68.9	328%

with a critical axial compression ratio. Many scholars have found that the cracking strength of rock is generally (0.3 ~ 0.4) σ_c, so with the critical axial compression ratio being beyond this range, a certain degree of damage has occurred in the rock (Xue et al. 2014). It can be seen that the corresponding principal stress axis rotation angle when sandstone failed under the axial–torsional test was closely related to the initial stress state of the rock.

Before conducting the analysis, we have to understand two basic consensuses.

1) The loading process of the rock satisfies the law of conservation of energy—that is, the axial stress applied by the loading device to the specimen is a process of continuous work, and this part of the energy is stored in the specimen in the form of elastic energy.
2) The propagation direction of microcracks in the rock is closely related to the orientation of the principal stress (Diederichs et al. 2004; Eberhardt 2001).

Based on the above, we know that when the applied axial stress is low—that is, when the energy stored in the rock is small—the primary microcracks inside the rock are compacted, the density of the microcracks is significantly reduced, and the ability to resist deformation is enhanced. At this stage, stress with a larger change in orientation can cause the microcracks to penetrate and eventually lead to the destruction of the rock. As the internal energy of the rock increases, until it exceeds the cracking strength of the rock, microcracks of different lengths and directions within the rock rapidly sprout and expand, and the internal damage of the sample intensifies, the ability to resist deformation being gradually lost. At this stage, a small rotation angle of the stress axis can aggravate the interpenetration of microcracks and cause damage to the specimen. Regardless of the initial degree of damage, the rotation of the principal stress axis aggravates the deformation and failure of the rock. However, the initial degree of damage affects the strength of the stress axis rotation aggravating impact. The greater the initial degree of damage, the stronger the aggravating effect, and vice versa.

Based on the above analysis, the author believes that the critical axial compression ratio can be used to determine the strength of the stress principal axis rotation aggravating effect. When the axial compression ratio of the rock exceeds the critical value, a small rotation of the principal stress axis causes larger deformation and severe damage to the rock. At this stage, it is necessary to strengthen the monitoring of the change in the rock stress direction and take timely measures to maintain rock stability. The discovery of the laws mentioned above has improved our understanding of the properties of rock mechanics, providing important theoretical support for the safe and effective construction of rock engineering.

Table 4 The relationship between the axial compression ratio and principal stress rotation angle

Rock types	Fitting formula	Fitting coefficient
Red sandstone	$\alpha = 11.2 + 23.96 \bullet 0.04^n$	0.93
White sandstone	$\alpha = 8.69 + 33.73 \bullet 0.1^n$	0.99
Gray sandstone (fine)	$\alpha = 13.96 + 24.65 \bullet 0.05^n$	0.93
Gray sandstone (coarse)	$\alpha = 12.19 + 29.26 \bullet 0.12^n$	0.99

Mechanism of rock fracture evolution under rotation of principal stress axis

As early as 2001, Eberhardt (2001) performed a three-dimensional numerical simulation of tunnel excavation and found that the rotation angle of the principal stress axis controlled the direction of crack propagation and proposed a crack propagation model considering this (see Fig. 8). Although scholars have discussed the relationship between principal stress axis rotation and rock mechanics based on

Table 5 Critical axial compression ratio of four sandstones

Rock types	σ_c/MPa	p/MPa (Critical value)	σ_z/MPa (Critical value)	n
Red sandstone	40	5	15	0.38
White sandstone	36	8	24	0.67
Gray sandstone (fine)	90	16.6	49.8	0.55
Gray sandstone (coarse)	70	10	30	0.43

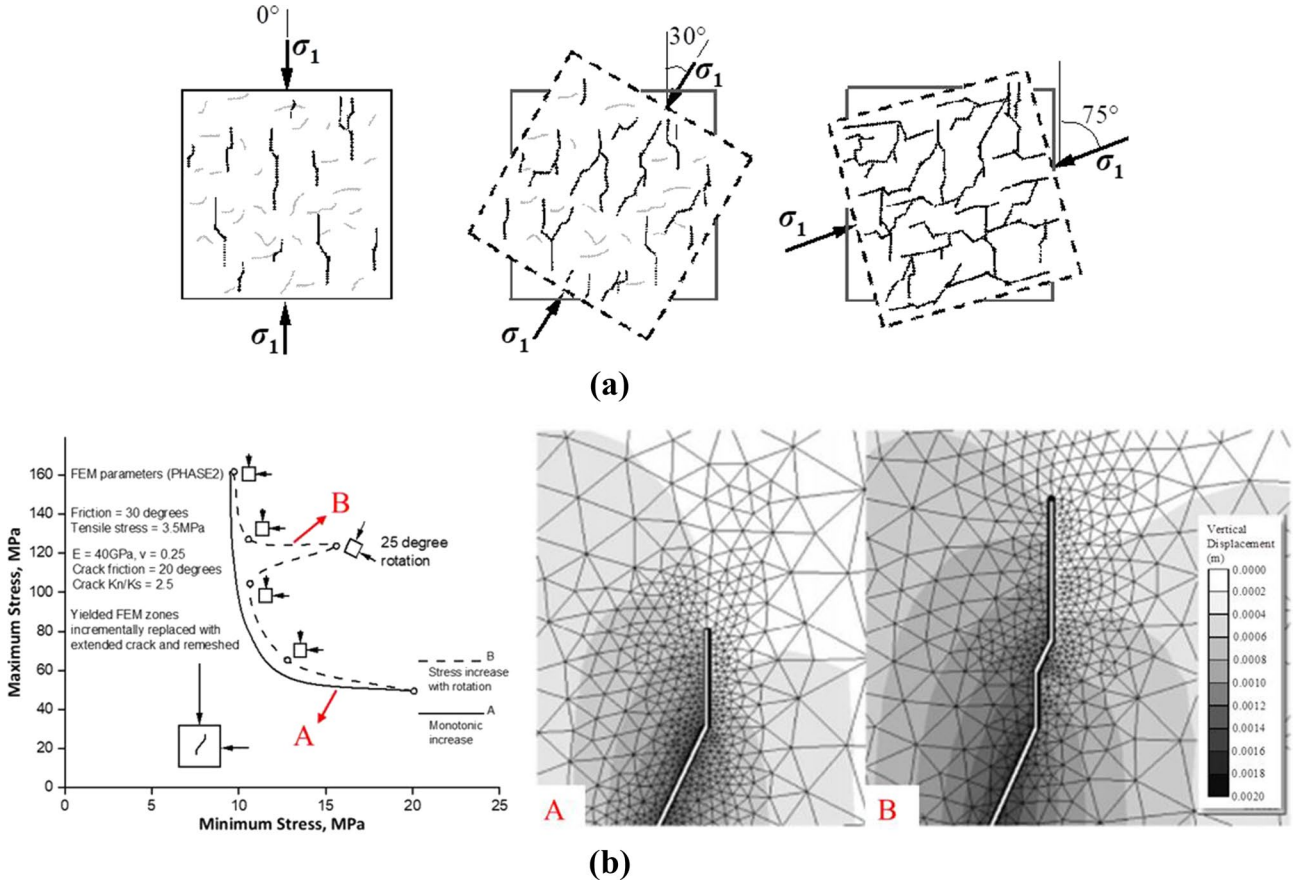

Fig. 8 Crack growth model considering the rotation of the principal stress axis (Eberhardt 2001): **a** crack propagation model caused by maximum principal stress rotation; **b** simulation of the crack propagation process caused by the principal stress rotation (A, the magnitude of the stress changes only; B, the magnitude and direction of the stress change at the same time)

the model for two decades (Diederichs et al. 2004; Zhang and Liang 2007; Cui and Wang 2014), little research has been conducted on the verification of rock mechanics. In this study, based on the relationship between the fracture angle of sandstone and the rotation angle of the principal stress axis under the axial–torsional test (Fig. 9), the evolution mechanism of the internal fractures in the rock is explored. The fracture angle in curves refers to the angle between the fracture surface and the vertical direction, the rotation angle is the angle between the maximum principal stress and the vertical direction when the rock fails.

In Fig. 9, the fracture angles of the four sandstones under different axial stresses have a specific correlate with the rotation angle of the principal stress axis, but the specific changes differ slightly. With an increase in axial stress, the fracture angle of red sandstone and white sandstone gradually changes from the rotation angle of the principal stress axis to greater than the rotation angle. Using white sandstone as an example, when the axial stress is lower than 24 MPa, the fracture angle is approximately the same as the rotation angle; conversely, when the axial stress is higher than 24 MPa, the fracture angle is larger than the rotation angle. Coincidentally, this critical value is consistent with what was obtained in Sec. 3.1. Based on the above analysis, it can be seen that when the axial stress is lower than 24 MPa, the cracks in the rock are in a stable state. At this stage, the damage of the rock is dominated by the rotation of the principal stress axis, so the fracture angle of the specimen is consistent with the rotation angle. When the axial stress is higher than 24 MPa, the internal cracks of the rock are unstable. Its expansion depth and density change significantly under the rotation of the principal stress axis. The rock fails at a small rotation angle, the fracture angle being larger than the rotation angle. At this stage, the rotation of the principal stress axis accelerates the crack propagation of the rock and intensifies the failure process.

With an increase in axial stress, the fracture angle of coarse gray sandstone gradually changes from the rotation angle of the principal stress axis to less than the rotation angle. This feature can be explained as follows—coarse gray

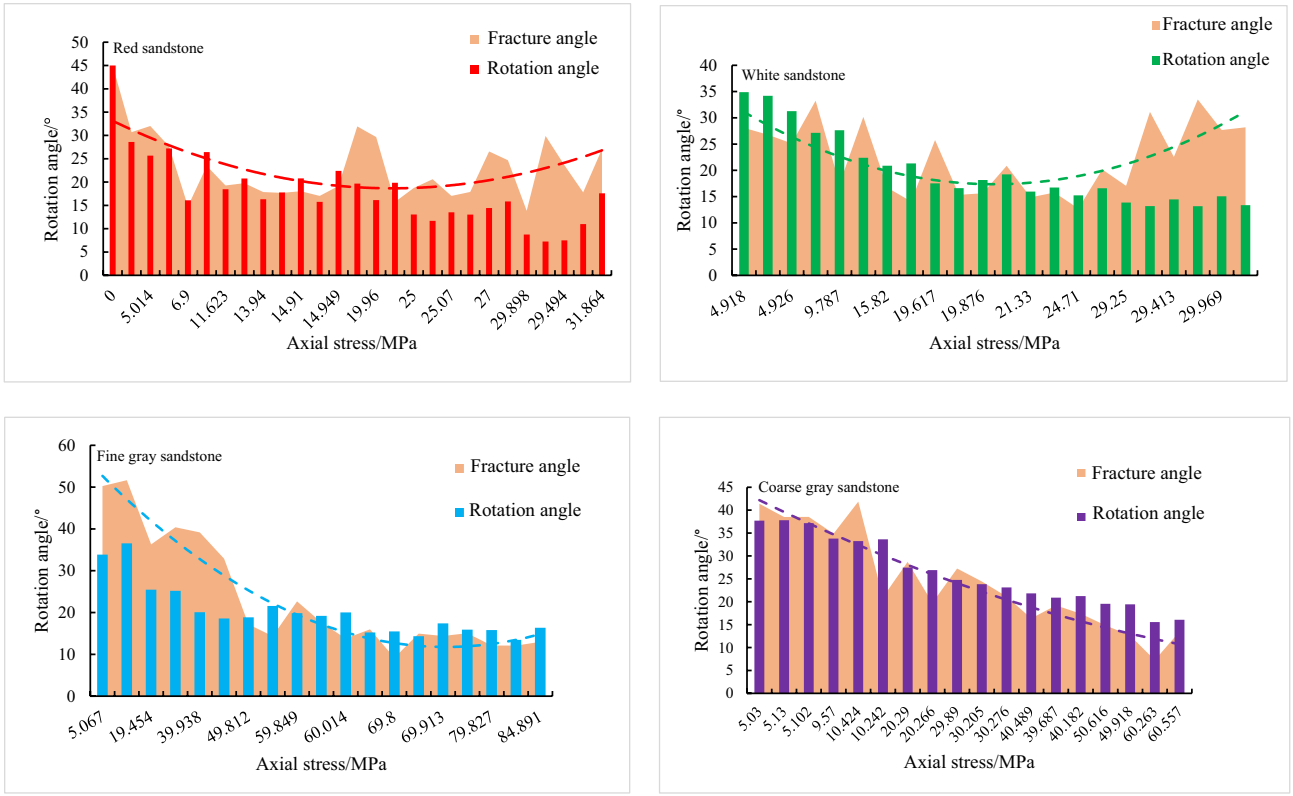

Fig. 9 Curves of fracture angle VS principal stress rotation angle of sandstones under axial–torsional test

sandstone being more brittle than white sandstone. When the applied axial stress is close to the uniaxial compressive strength of the rock, significant damage occurs inside the rock, and there are many vertical tensile cracks. Considering that crack growth is not simply based on its extending direction, the optimal direction selected is based on the interaction of adjacent microcracks (Xu et al. 1986). Consequently, the rotation of the principal stress plays a role in aggravating the penetration between cracks. Finally, coarse gray sandstone exhibits a tensile-shear failure mode.

The fracture angle of fine gray sandstone gradually changes from significantly greater than the rotation angle to slightly less than the rotation angle with an increase in the axial stress. The changing trend differs slightly from red sandstone, white sandstone, and coarse gray sandstone. The author speculates that this phenomenon is related to the internal composition of the rock. As shown in Fig. 10, the internal pores of the coarse-grained structure are large and few, while the internal pores of the fine-grained structure are tiny and many. From the

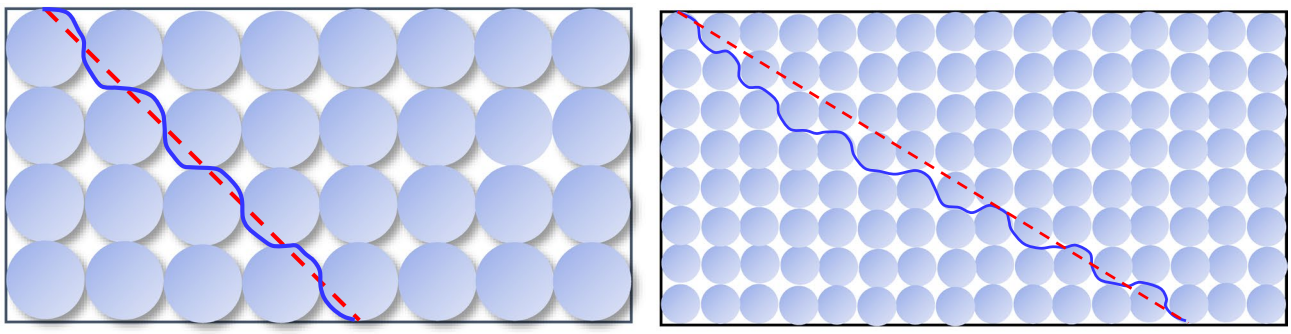

Fig. 10 Schematic diagram of fracture evolution path of rock grain structure: **a** schematic diagram of coarse grain structure; **b** schematic diagram of fine grain structure

perspective of energy, crack propagation in rock is a process of energy dissipation, the crack continually propagates along the path with less energy dissipation, which generally occurs at the boundary between particles and cement (Xu et al. 1986). In the coarse-grained structure, owing to the large particle size and more cementitious materials filled between particles, the crack propagation path is relatively short. This means that under lower axial stress, the corresponding fracture angle of the rock failure is consistent with the rotation angle of the principal stress axis. For the fine-grained structure, owing to the large specific surface area between the particles, the crack propagation path is relatively long, the entire process dissipating more energy. Finally, the fracture angle is greater than the rotation angle. The compactness and strength of white sandstone, red sandstone, coarse gray sandstone, and fine gray sandstone increase in turn. Under lower axial stress, the relationship between the corresponding fracture angle and the rotation angle gradually changes from consistent to a fracture angle greater than the rotation angle.

In summary, the different internal composition of the four sandstones leads to the relationship between the fracture angle and the rotation angle slightly different. However, the change law between them reflects the same fracture propagation mode under the rotation of the principal stress axis. That is, the propagation direction of the crack tip is parallel to the principal stress orientation and deflects with the rotation of the principal stress axis, expands, and even penetrates one another, finally leading to rock failure. It should be noted that the final failure mode of rock is caused by the joint action of the internal composition and structure of the rock, distribution of primary fractures, the rotation angle of the principal stress axis, and other factors.

Consequently, the rock failure law obtained in this study not only confirms the crack propagation model considering the rotation of the principal stress axis proposed by predecessors, but also further refines the relationship between the model and the rock stress state, providing a reliable basis for popularization and application.

Conclusions

The strength, deformation, and failure characteristics of sandstone under the continuous rotation of the principal stress axis were studied through a series of axial–torsional tests on four types of sandstone. Based on the test results, the following conclusions were obtained:

1) According to the stress curves of sandstones, the effect of principal stress axis rotation on the peak strength is analyzed. The results show that the peak strength of different sandstones under the axial–torsional test has a nonlinear positive correlation with the axial stress and a negative correlation with the rotation angle of the principal stress axis.
2) The generalized-shear-stress–generalized-shear-strain curves describe the evolution of rock crack propagation under axial–torsional test, which can be divided into four stages: initial compaction stage, elastic stage, yield stage, and strain softening stage. Moreover, the yield platform and deformation modulus increase with the axial stress.
3) By applying different axial stresses, the effect of the initial damage degree of sandstones considering the principal stress rotation is explored. It is found that the rotation of principal stress axis intensifies the deformation and failure of rock, especially when the axial compression ratio exceeds the critical value. This critical value can be calculated from the initiation strength of the rock. Specifically, when the axial compression ratio of the rock is greater than the critical value—that is, when the initial degree of damage is large—the rotation of the principal stress axis at a small angle will lead the rock to be damaged severely. At this stage, certain measures such as surrounding rock support and avoidance disturbance should be taken to mitigate the effects.
4) The mechanism of rock fracture evolution is analyzed under the rotation of the principal stress axis based on rock failure characteristics. The results show that the rotation of the principal stress axis affected the expansion direction of the internal cracks in the rock, which intensified the expansion and penetration of the cracks to a certain extent. The applicability of the crack propagation model considering stress principal axis rotation is verified, and it is believed that the final rock failure shape is not only affected by the principal stress axis rotation, but also the internal composition structure of the rock, and the distribution of primary fractures.

Acknowledgements The authors would like to thank the financial supports provided by National Natural Science Foundation of China (NSFC) (42102307, 52009128); Open Research Fund of State Key Laboratory of Geomechanics and Geotechnical Engineering, Institute of Rock and Soil Mechanics, Chinese Academy of Sciences Grant (Z2019023); Natural Science Foundation of Jiangsu Province (BK20209992); and Jiangsu Province High-level Innovative and Entrepreneurial Talent Introduction Plan. Besides, the authors are also grateful to the anonymous reviewers for their careful reading of our manuscript and their many helpful comments.

Data Availability The data that support the findings of this study are available from the corresponding author, Hui Zhou (hzhou@whrsm.ac.cn), upon reasonable request.

Declarations

Competing interests The authors declare no competing interests.

References

Abel JF, Lee FT (1973) Stress changes ahead of an advancing tunnel. Int J of Rock Mech Min Sci 10(6):673–697

Alsayed MI (2002) Utilising the Hoek triaxial cell for multiaxial testing of hollow rock cylinders. Int J Rock Mech Min Sci 39(3):355–366

Cui W, Wang N (2014) Principal stress axis rotation and effect on failure model of surrounding rock during tunnelling. J Cent South Univ (Sci Tech) 45(6):2062–2070 **(in Chinese)**

Diederichs MS, Kaiser PK, Eberhardt E (2004) Damage initiation and propagation in hard rock during tunneling and the influence of near face stress rotation. Int J Rock Mech Min Sci 41(5):785–812

Diederichs MS (2000) Instability of hard rock masses: the role of tensile damage and relaxation. PhD thesis, University of Waterloo. http://hdl.handle.net/10012/480

Dunning J, Douglas B, Miller M, Mcdonald S (1994) The role of the chemical environment in frictional deformation: stress corrosion cracking and comminution. Pure Appl Geophys 143(1):151–178

Eberhardt E (2001) Numerical modeling of three-dimensional stress rotation ahead of an advancing tunnel face. Int J Rock Mech Min Sci 38(4):499–518

Feng XT, Chen SL, Zhou H (2004) Real-time computerized tomography (CT) experiments on sandstone damage evolution during triaxial compression with chemical corrosion. Int J Rock Mech Min Sci 41(2):181–192

Feucht LJ, Logan JM (1990) Effects of chemically active solutions on shearing behavior of a sandstone. Tectonophysics 175(1/3):159–176

Hight D, Gens A, Symes M (1983) The development of a new hollow cylinder apparatus for investigating the effects of principal stress rotation in soils. Geotechnique 33(4):355–383

Hu DW, Zhou H, Zhang F, Shao JF (2010) Evolution of poroelastic properties and permeability in damaged sandstone. Int J Rock Mech Min Sci 47(6):962–973

Hu SC, Tan YL, Zhou H, Guo WY, Hu DW, Meng FZ, Liu ZG (2017) Impact of bedding planes on mechanical properties of sandstone. Rock Mech Rock Eng 50:2243–2251

Jiang Y, Zhou H, Lu JJ, Gao Y, Zhang CQ, Chen J (2019) Analysis of stress evolution characteristics during TBM excavation in deep buried tunnels. Bull Eng Geol Environ 78:5177–5194

Jiang Y, Zhou H, Lu JJ, Gao Y (2023) Experimental study of hollow-cylinder sandstone under constant mean stress considering the rotation of principal stress axes. Rock Mech Rock Eng 56:3231–3238. https://doi.org/10.1007/s00603-022-03197-9

Kaiser PK, Yazici S, Maloney S (2001) Mining induced stress change and consequences of stress path on excavation stability: A case study. Int J Rock Mech Min Sci 38(2):167–180

Lee DH, Juang CH, Chen JW, Lin HM, Shieh WH (1999) Stress paths and mechanical behavior of a sandstone in hollow cylinder tests. Int J Rock Mech Min Sci 36:857–870

Li XB, Zhou ZL, Lok TS, Huang L, Yin TB (2008) Innovative testing technique of rock subjected to coupled static and dynamic loads. Int J Rock Mech Min Sci 45(5):739–748

Li XB, Fengqiang G, Ming T, Dong Longjun Du, Kun MC, Zilong Z, Tubing Y (2017) Failure mechanism and coupled static-dynamic loading theory in deep hard rock mining: a review. J Rock Mech Geotech Eng 9(4):767–782

Li T, Pei X, Guo J, Meng M, Huang R (2020a) An energy-based fatigue damage model for sandstone subjected to cyclic loading. Rock Mech Rock Eng 53:5069–5079

Li M, Wang D, Shao Z (2020) Experimental study on changes of pore structure and mechanical properties of sandstone after high-temperature treatment using nuclear magnetic resonance. Eng Geol 275:105739. https://doi.org/10.1016/j.enggeo.2020.105739

Logan JM, Blackwell MI (1983) The influence of chemically active fluids on frictional behavior of sandstone. EOS, Trans Am Geophys Union 64(2):835–837

Qian QH, Li SC (2008) A review of research on zonal disintegration phenomenon in deep rock mass engineering. Chin J Rock Mech Eng 27(6):1278–1284 (in Chinese)

Sayao A, Vaid Y (1991) A critical assessment of stress nonuniformities in hollow cylinder test specimens. Can Geotech J 31(1):60–72

Vaid Y, Sayao A, Hou E et al (1990) Generalized stress-path-dependent soil behaviour with a new hollow cylinder torsional apparatus. Can Geotech J 27(5):601–616

Wang S, Xu W, Jia C, Wang W (2017) Mechanical behavior of fine-grained sandstone in triaxial compression and elastoplastic modeling by return mapping algorithms. Bull Eng Geol Environ 77:1689–1699

Wasantha PLP, Ranjith PG, Zhao J, Shao SS, Permata G (2015) Strain rate effect on the mechanical behaviour of sandstones with different grain sizes. Rock Mech Rock Eng 48:1883–1895

Xu P, Yang SQ (2016) Permeability evolution of sandstone under short-term and long-term triaxial compression. Int J Rock Mech Min Sci 85:152–164

Xu J, Li H, Xian XF, Yin GZ (1986) Meso-mechanical experiment of micro fracturing progress of sandstone under uniaxial stress condition. Mech Eng 8(4):16–20 (in Chinese)

Xue L, Qin SQ, Sun Q, Li WC (2014) A study on crack damage stress thresholds of different rock types based on uniaxial compression tests. Rock Mech Rock Eng 47:1183–1195

Yang SQ (2016) Experimental study on deformation, peak strength and crack damage behavior of hollow sandstone under conventional triaxial compression. Eng Geol 213:11–24

Yang SQ, Jing HW (2013) Evaluation on strength and deformation behavior of red sandstone under simple and complex loading paths. Eng Geol 164:1–17

Yang SQ, Jing HW, Wang SY (2012) Experimental investigation on the strength, deformability, failure behavior and acoustic emission locations of red sandstone under triaxial compression. Rock Mech Rock Eng 45:583–606

Yang SQ, Ranjith PG, Gui YL (2015) Experimental study of mechanical behavior and X-ray micro CT observations of sandstone under conventional triaxial compression. Geotech Test J 38(2):179–197

Yang SQ, Xu P, Li YB, Huang YH (2017) Experimental investigation on triaxial mechanical and permeability behavior of sandstone after exposure to different high temperature treatments. Geothermics 69:93–109

Yi C, Johansson D, Greberg J (2017) Effects of in-situ stresses on the fracturing of rock by blasting. Comput Geotech 104(DEC.):321–330

Zhang SR, Liang LH (2007) Analysis on tunnel liner supporting time considering three-dimensional stress rotation. J Hydrol Eng 38(6):704–709 **(in Chinese)**

Zhang C, Zhou H, Feng X, Xing L, Qiu S (2013) Layered fractures induced by principal stress axes rotation in hard rock during tunnelling. Mater Res Innov 15(sup1):527–530

Zhou H, Jiang Y, Lu JJ, Gao Y, Chen J (2018a) Development of a hollow cylinder torsional apparatus for rock. Rock Mech Rock Eng 51:3845

Zhou H, Jiang Y, Lu JJ, Hu DW, Zhang CQ, Chen J, Li Z (2018) Study of hollow cylinder torsional apparatus for rock. Rock Soil Mech 40(5):1917–1922 (in Chinese)

Zou D, Kaiser PK (1990) Determination of in situ stresses from excavation-induced stress changes. Rock Mech Rock Eng 23(3):167–184